A topological screening heuristic for low-energy, high-index surfaces

Wenhao Sun [a,b,*], Gerbrand Ceder [a,b,c]

[a] *Materials Sciences Division, Lawrence Berkeley National Laboratory, Berkeley, CA 94720, USA*
[b] *Department of Materials Science and Engineering, Massachusetts Institute of Technology, Cambridge, MA 02139, USA*
[c] *Department of Materials Science and Engineering, UC Berkeley, Berkeley, California 94720, USA*

ARTICLE INFO

ABSTRACT

Robust *ab initio* investigations of nanoparticle surface properties require a method to identify candidate low-energy surface facets *a priori*. By assuming that low-energy surfaces are planes with high atomic density, we devise an efficient algorithm to screen for low-energy surface orientations, even if they have high (hkl) miller indices. We successfully predict the observed low-energy, high-index $\{10\bar{1}2\}$ and $\{10\bar{1}4\}$ surfaces of hematite α-Fe_2O_3, the $\{311\}$ surfaces of cuprite Cu_2O, and the $\{112\}$ surfaces of anatase TiO_2. We further tabulate candidate low-energy surface orientations for nine of the most common binary oxide structures. Screened surfaces are found to be generally applicable across isostructural compounds with varying chemistries, although relative surface energies between facets may vary based on the preferred coordination of the surface atoms.

© 2017 Published by Elsevier B.V.

1. Introduction

Many important interfacial properties of nanoparticles, such as reactivity [1], photocatalytic activity [2], crystal-growth direction [3], and intercalation rates for battery electrodes [4], depend on which surface facets are exposed on the particle morphology. At equilibrium, this morphology is given by the Wulff construction, which can be predicted from first-principles by calculating which surface orientations bound the nanocrystal with the lowest surface energy. This process determines which surfaces are stable, and are therefore relevant for more sophisticated investigations of surface properties or reactions. The first step in an *ab initio* investigation of nanoparticle interfacial properties is the selection of which surface orientations to calculate. Ideally, one would choose the stable surface facets observed in experimental nanoparticle morphologies, but when these are unavailable, surface investigations have typically been constrained to the low-index surfaces (Miller indices hkl all being either 0 or $\pm$ 1). However, particle morphologies can often exhibit stable high-index surfaces, such as the $\{10\bar{1}2\}$ and $\{10\bar{1}4\}$ surfaces of rhombohedral crystals such as hematite Fe_2O_3 [5] and Calcite $CaCO_3$ [6]. High-index surfaces can also be stabilized electrochemically, as in the (730) surfaces of FCC platinum [7], or via adsorbates, such as the (311) surfaces of cubic Cu_2O [8]. Most surface properties are strongly orientation-dependent, so if stable high-index surfaces are not considered in a computational investigation, then calculated surface properties may be largely irrelevant.

One might consider searching for low-energy, high-index surface orientations by calculating the energy of surfaces attained by a brute force enumeration of surface orientations [9]. However, this process can be combinatorically prohibitive, as combinations of Miller indices up to index N yield $O(N^3)$ surface orientations, each with potentially multiple unique terminations. It can also be wasteful, as usually only a small handful of surface facets are energetically competitive to appear on the Wulff construction. Furthermore, it may actually be conceptually flawed to search for low-energy surfaces by Miller index, as Miller indices are defined with respect to the conventional unit-cell lattice, which is not unique, and is a 'human' convention, rather than a physical one. Atomic positions are a physically-relevant crystallographic feature to search for low-energy surfaces by, but the lattice does not include this information.

In this paper, we propose an efficient, physically-motivated screening heuristic for low-energy surfaces that does not depend on how the unit-cell is defined. Our heuristic is based on the hypothesis that low-energy surfaces tend to be planes with high atomic density. This is a reasonable assumption for two reasons: 1) because planes with greater atomic density have the potential for more in-plane bonds, which reduces the surface energy. 2) The Gibbs-Thomson model relates excess chemical potential to plane curvature, indicating that flat planes have the lowest free-energy. While this argument is generally exercised at the microscopic level, the geometric argument operates on a similar principle at the atomic level.

Our heuristic is described as follows. Planes can be defined by any set of three atoms. By identifying all the possible unique planes formed by sets of three atoms within a crystal structure, and identifying which Miller indices are most highly represented by this survey, we identify the highest-density planar orientations, which are promising candidates

---
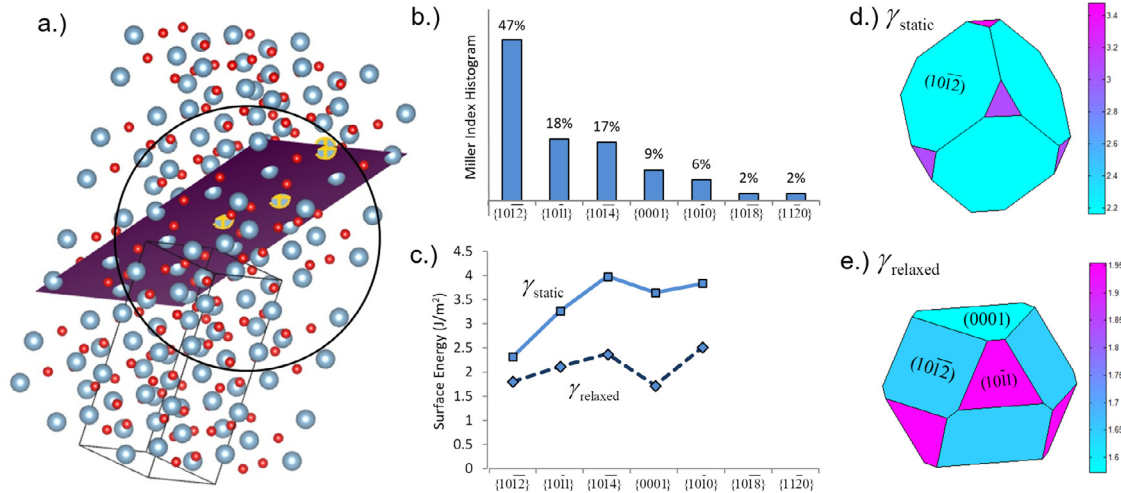
Fig. 1. The low-energy, high-index surface screening heuristic a.) Surface orientations are sampled by enumerating triplets of atoms in a sphere around the symmetrically-distinct atoms in a unit cell. b.) The frequency of sampled orientations is collected in a histogram, where highly sampled surfaces correspond to greater planar atomic densities, shown for the corundum α-Al_2O_3 structure. c.) Static and relaxed surface energies of orientations obtained using the screening heuristic. Greater atomic planar densities generally correlate with lower surface energies. d.) Wulff construction from static surface energies. e.) Wulff construction made from relaxed surface energies.

for the lowest-energy surfaces. Our proposed algorithm is successful at identifying multiple observed low-energy, high-index planes for several important oxide structures. Because our algorithm is based on the crystal structure, but not the chemistry, we perform an analysis for the applicability of screened surfaces across isostructural compounds with varying chemistries, and how chemistry changes the relative surface energies between facets. Our screening heuristic is powerful and computationally inexpensive, and should precede any *ab initio* investigation of surface properties where the equilibrium particle morphology is unknown.

2. Methodology

We aim to develop a quantitative descriptor for high-density planes that is easy to identify computationally, and does not require explicit construction of surface slabs to achieve. We begin by reasoning that a complete sampling of planes formed by three atoms will naturally be biased towards surface orientations with high-density. Here, we start with a description of the algorithm, illustrated in Fig. 1a, including a discussion of subtleties to be aware of in order to minimize the identification of spurious high-index surfaces.

1. **For a given unit cell, identify all symmetrically unique atoms.** This eliminates the dependence of the algorithm on the orientation of the chosen lattice, or the number of primitive unit cells within this orientation. This further ensures that environments of atoms on high-symmetry Wyckoff positions are not oversampled.
2. **For each symmetrically unique atom, construct a sphere of cut-off radius r_0.** The radius of this sphere should encompass enough atoms to attain a reasonable sampling of the local short-range atomic environment. The number of triplets of atoms scales as $_NC_2$, where N is the number of atoms in the sphere. We find that an r_0 that encompasses 50 atoms is sufficient to identify most low-energy high-index surfaces.
3. **Within this sphere, identify all sets of three atoms that include the original atom.** In the cases of complex ions, such as $CO_3{}^{2-}$, $SO_4{}^{2-}$, $PO_4{}^{3-}$, $AlH_4{}^-$, $NH_4{}^+$, etc, only the center atom is considered. If all atoms are considered for these cases, then surface orientations representing the surfaces of ionic polyhedra become oversampled, rather than just the preferred cleavage surfaces of the cationic/anionic sublattice.
4. **Determine the Miller indices of the plane formed by the sets of three atoms**, defined with respect to the desired unit cell, which is typically the conventional one. To do this generally, for Bravais

lattices of any symmetry, one begins by forming two vectors from the three atoms. The Miller indices of the *vectors* can be found from $v_{\text{Miller}} = L^{-1}v$ where L is the lattice of the desired unit cell, and v is the vector formed between two of the three atoms, defined with respect to the same standard basis as the lattice. The Miller index of the plane formed by these two vectors is the cross product of the two Miller vectors. Miller indices with irreducible fractional indices are discarded, as one cannot create a slab with irreducible fractional indices that satisfies periodic boundary conditions.

5. **Build a histogram of sampled surface orientations. The orientations that occur the most frequently are the ones with the greatest planar atomic density.** Miller indices that are equivalent by symmetry (i.e. in a family) should be grouped together. The family of a Miller index can be constructed by applying all the point group operations of the reciprocal lattice to the Miller index.

We next apply this surface screening algorithm to a selection of binary oxides that have been experimentally observed to exhibit high-index surfaces. We compute the surface energy, γ, using the equation

$$\gamma = \frac{1}{2A}\left(E_{slab} - N E_{bulk}\right) \tag{1}$$

where A is the area of the surface unit cell, E_{slab} is the energy of the slab supercell, E_{bulk} is the bulk energy per atom, and N is the number of atoms in the surface slab. The $\frac{1}{2}$ pre-factor accounts for the two surfaces of a slab. If the surface can exchange molecular or atomic species with an external reservoir, then the surface grand potential is:

$$\gamma = \frac{1}{2A}\left(E_{slab} - N E_{bulk} - \sum_i N_i \mu_i\right) \tag{2}$$

where excess or deficient atoms are accounted for by a chemical potential term for the N_i atoms of species i with chemical potential μ_i.

For this work we only consider stoichiometric oxide surface slabs, constructed from planar cleavages of a bulk crystal, where the surface energy is given by Eq. (1). In real oxide surfaces, surface reconstructions may occur, where the surface structure changes to accommodate the energetic cost of broken bonds [10]. Surfaces may also become non-stoichiometric under highly oxidizing or reducing oxygen environments, changing the surface energy according to Eq. (2), thereby influencing which surface facets appear on the equilibrium morphology [11,12]. Although explicit calculations of non-stoichiometric or reconstructed surfaces are beyond the scope of this work, we will demonstrate that the surface orientations screened using our planar-density heuristic are

often experimentally observed to be stabilizable under applied environmental conditions. In other words, our screened surface orientations can identify high-density surfaces that may be unstable in a cleanly-cleaved form, but have the potential to be stabilized when accounting for non-stoichiometry or reconstructions. This highlights the advantage of using a screening metric based on the underlying structural topology of the crystal, rather than on the specific cleavages and reconstructions of an explicit surface structure.

To calculate surface energies, we prepare surface slabs using the efficient creation and convergence scheme we previously derived in [13]. In this scheme, bulk unit cells are first reoriented such that the (001) basal plane lies parallel to the Miller plane of interest. A surface slab is next generated by inserting a vacuum into a supercell extended along the [001] vector. We rapidly converge the surface energy with respect to slab thickness by using an E_{Bulk} in Eq. (1) computed from a bulk unit cell oriented in the same direction as the surface slab, which minimizes numerical errors arising from Brillouin zone integration across different lattices.

All calculations were performed using the Vienna Ab-Initio Software Package (VASP). We used the projector augmented wave (PAW) [14] method with the Perdew–Burke–Erzhenhoff (PBE) [15] generalized-gradient approximation. Plane-wave basis cutoff energies were calculated at 520 eV cutoff energy. Brillouin Zones were sampled using the Methfessel–Paxton scheme. Bulk unit cells and atoms were initially relaxed until forces were 1E−6 eV/Å. Surface slabs were then created from relaxed bulk unit cells to be at least 15 Å thick with 12 Å of vacuum. No Hubbard+U term is utilized for the transition metal oxide surfaces, as we find it to occasionally lead to convergence issues when the slab is relaxed; possibly related to the multiple-minima issue of DFT+U [16]. A python implementation of this screening algorithm is provided in the supplemental information, based on the Python Materials Genomics (*pymatgen*) package [17].

3. Validation

3.1. Corundum Al₂O₃

To demonstrate our surface screening heuristic, we first test it on the α-Al$_2$O$_3$ corundum structure (space group $R\bar{3}c$, #167), whose equilibrium morphology is dominated by the high-index $\{10\bar{1}2\}$, and low-index $\{10\bar{1}1\}$ and $\{0001\}$ surfaces [18]. The $\{10\bar{1}4\}$ surface is also a prominent surface in this structure, as $\{10\bar{1}4\}$ cuts of α-Al$_2$O$_3$ can be used as substrates for crystal growth [19], and the isostructural α-Fe$_2$O$_3$ hematite structure can been synthesized hydrothermally to be completely bounded by $\{10\bar{1}4\}$ surfaces [20]. We show the results of our surface screening heuristic in Fig. 1b, finding that triplets of atoms sample the $\{10\bar{1}2\}$ surfaces the most frequently, at 47% of the time, followed by $\{10\bar{1}1\}$ and $\{10\bar{1}4\}$ with 18% and 17% each, and then the low-index $\{0001\}$ with 9% and $\{10\bar{1}0\}$ with 6%. The $\{10\bar{1}8\}$ and $\{11\bar{2}0\}$ surfaces are also identified, but each only occurring with 2% frequency. Such screened surfaces with low occurrences may merit investigation, but are generally less relevant.

If our heuristic is valid, then the most highly screened surfaces should, in general, yield the lowest surface energies. To validate our hypothesis, we calculate the static and relaxed surface energies of the aforementioned corundum surfaces. We successfully find a strong correlation showing that surfaces that are screened with high probabilities tend to have lower surface energies, and validate that the high-index $\{10\bar{1}2\}$ surface has the lowest surface energy of all orientations (Fig 1c). The structure of the $\{10\bar{1}2\}$ surface is given in Fig. 2a, showing that all surface Al atoms are 5-fold coordinated, and the O atoms are 3-fold coordinated. This Al coordination is nearly the same as in the bulk (6-fold), yielding structural insight on why this is such a low-energy surface. On the other hand, the $\{10\bar{1}0\}$ surface shows mixed 5-fold and 4-fold coordinated Al, and the $\{10\bar{1}4\}$ surface is completely composed of 4-fold coordinated cations (Fig. 2b). The conventional wisdom that high-index

Table 1
Heuristic screened Cu$_2$O surfaces and resulting surface energies in (J/m^2). Polar surfaces marked by an asterisk*, and are calculated by a Tasker 3 to Tasker 2b reconstruction, neutralizing the dipole by moving half the Cu atoms to the other side of the slab.

Surface	Screening	γ_{static}	γ_{relax}
(111)	21%	0.80	0.75
(100)*	17%	1.58	1.22
(110)*	13%	1.70	1.39
(311)	12%	1.44	1.04
(210)*	7.8%	1.38	1.06
(331)	7.0%	1.08	0.89

surfaces possess more step-edges and kinks may be true for the vicinal surfaces of simple metals, but our findings demonstrate that for more complicated crystal structures, high-index surfaces can be as atomically flat as low-index surfaces, or even more so.

The $\{0001\}$ surface of Al$_2$O$_3$ is only sampled by 9% of triplets of atoms, and accordingly, the static surface energy is higher than for $\{10\bar{1}0\}$, although not as high as the $\{10\bar{1}4\}$. However, relaxation greatly reduces the surface energy of the $\{0001\}$ surface, turning it from a minority facet on the α-Al$_2$O$_3$ particle morphology to a primary facet (Fig. 1d,e). Because the surface screening heuristic is applied to the *bulk* crystal, information regarding the screened surfaces will be most relevant for static surface energies. While some surfaces, such as the Al$_2$O$_3$ $\{0001\}$, will relax more heavily than others, surfaces with low γ_{static} will still tend to have low γ_{relax}, so surfaces attained by the heuristic should always be considered as candidate surfaces in an *ab initio* investigation.

Finally, to provide a counterpoint to our screening heuristic, we further calculate the remaining low-index surfaces for α-Al$_2$O$_3$, namely, the $\{10\bar{1}1\}$ and the $\{11\bar{2}1\}$, as well as the high-index $\{11\bar{2}3\}$ surface, which was proposed to be a stable facet from angle measurements on the particle morphology. The static (and relaxed) surface energies for these surfaces are, respectively, 3.57 (2.19) J/m^2, 4.1 (3.02) J/m^2, and 5.13 (3.30) J/m^2. These values are similar to the highest surface energies of the screened surfaces, suggesting that surfaces attained from our screening heuristic are probably better starting points than a low-index surface enumeration.

Seven binary oxides are known to form in the corundum crystal structure – the group III semiconductor oxides Al$_2$O$_3$, Ga$_2$O$_3$, In$_2$O$_3$, as well as the transition metal oxides Ti$_2$O$_3$, V$_2$O$_3$, Cr$_2$O$_3$, and Fe$_2$O$_3$. In part III, we investigate whether or not surfaces screened on the basis of structure will remain valid as chemistry is altered.

3.2. Cuprite Cu₂O

We next study cubic Cu$_2$O, known as cuprite, a p-type semiconductor with a 2.17 eV band gap which has been identified as a promising candidate material for photocatalytic water splitting and for solar energy conversion [21]. Synthesis of Cu$_2$O within the presence of reducing agents can yield a rich diversity of crystalline morphologies. By increasing the concentration of the reductant NH$_2$OH$_3$•HCl, the relative area fraction of $\{100\}$, $\{110\}$, and $\{111\}$ surfaces can be tuned, with resulting nanoparticle shapes ranging from cubic to rhombic dodecahedral [22]. Recently, it was shown that when Cu$_2$O is synthesized under alkaline solution conditions with a D-(+)-glucose reducing agent, high-index $\{311\}$ surfaces of Cu$_2$O can be stabilized, enabling the formation of nanoparticles with over 50-facets [8]. These morphologies with high-index facets are of great interest, as the photocatalytic activity of Cu$_2$O nanoparticles improves substantially with an increasing number of facets. Other high-index surfaces for Cu$_2$O have been reported, proposed to be (211) and (744) surfaces [23], although these Miller indices are identified from angle measurements between facets, and may not be exact.
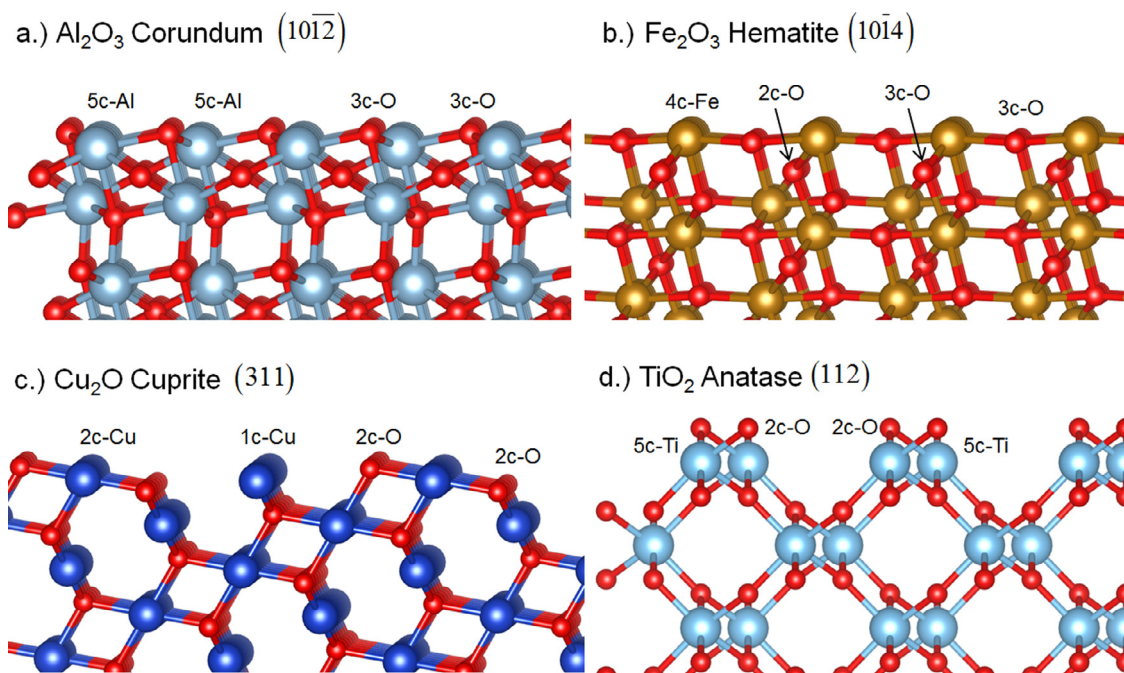
Fig. 2. Structures of low-energy, high-index surfaces for a.) Al$_2$O$_3$ corundum (10$\bar{1}$2), b.) Fe$_2$O$_3$ hematite (10$\bar{1}$4) c.) Cu$_2$O (311), and d.) TiO$_2$ anatase (112). High-index surfaces can be as atomically flat as low-index surfaces, or potentially even more so.

Application of our screening heuristic onto Cu$_2$O (Table 1) yields insight on the energetic competition between the surfaces for this structure, and the role of reducing agents in manipulating the crystal morphology and in stabilizing the high-index structures. From our screening, we find the low-index surfaces to be the most represented, in the order of the {111} planes at 21%, followed by the {100} with 17% and {110} with 13%. However, these low-index surfaces compose only 50% of the possible screened surfaces. Following these surfaces, we also find the {311} with 12%, {210} at 8%, and {331} planes at 7%, and after these, a large collection of other planar surfaces in this structure with <5% filling, including the polar {211}, {310}, and {320} surfaces, and the nonpolar {53$\bar{1}$} surface. The large number of candidate surfaces for this relatively simple structure, coupled with a fairly homogeneous sampling between multiple surface orientations, underlies the potential for this material to exhibit such a variety of particle morphologies.

Of these screened surfaces, surface energy calculations on stoichiometric slabs show the non-polar {111} and {311} surfaces to possess the lowest vacuum surface energies. The stoichiometric {100}, {110} and {210} surfaces are polar – consisting of alternating layers of 2-Cu$^+$ and O^{2-}. These polar surfaces, also known as Tasker Type-3 surfaces [24], have divergent electrostatic energies. In the lack of polarity-stabilizing mechanisms such as band structure charge transfer [25,26], these polar surfaces are classically unstable. For this reason, the experimentally-observed nanoparticle morphology in a solution with no reducing agents is dominated by the {111} surfaces, forming cubes [22]. When reducing agents are introduced, the oxygen-terminated surfaces of the polar {100} and {110} are likely etched in solution, screening the dipole and stabilizing these surfaces on the Wulff shape.

Following the low-index surfaces, the {311} surface is screened to be the next candidate surface. Our calculations confirm a low surface energy, although not low enough to appear on the vacuum Wulff morphology. This is consistent with observation, as the stabilization of the {311} surface requires both solution reducing conditions and stabilizing adsorbates. Nevertheless, our screening heuristic successfully identifies the potential for this particular surface orientation, out of all possible high-index surfaces, to be a low-energy surface. The surface structure of Cu$_2$O (311) is shown in Fig. 2c, showing a high planar density of copper atoms in the (311) plane. Like the high-index, low-energy corundum surfaces, the Cu$_2$O (311) demonstrates that high-index surfaces can be planar at the atomic scale. This suggests that the improved photocatalytic activity of Cu$_2$O nanocrystals with a large fraction of high-index surfaces does not necessarily originate from reactive steps-edges on vicinal surfaces. Instead, it may also arise from the increased number of edges and vertices where two planar faces meet, as these corner atoms are the least coordinated, and likely most reactive.
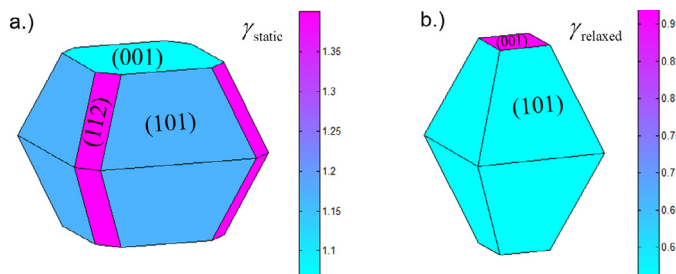
3.3. Anatase TiO$_2$

TiO$_2$ is a material of immense importance in the photocatalysis and geological communities [27,28]. At the nanoscale, the anatase structure is the thermodynamically stable phase, as it has the lowest surface energy of all its competing polymorphs [29]. Due to the importance of nanocrystalline TiO$_2$, there have been numerous theoretical and experimental investigations into the morphology of anatase TiO$_2$ surfaces and the photocatalytic properties of its surfaces [30,31]. Nearly all of these studies have focused on the low-index (001), (100), and (101) surfaces. However, nanoparticles of anatase TiO$_2$ formed via sol-gel methods under low pH conditions are often bound by {112} planes [28]. Under the presence of hydrofluoric acid and citric acid, anatase nanocrystals can also adopt a curved morphology consisting of quasi-continuous vicinal facets between the {101} and {112}, and under very high citric acid concentrations, the capping {001} surface can be destabilized with respect to a host of other high-index vicinal surfaces [32].

When we apply our topological screening heuristic on anatase TiO$_2$, we identify a surprisingly varied collection of candidate surface orientations for low-energy surfaces (Table 2). The {112} surface of anatase is actually identified to be the most prevalent surface orientation, with 18% occurrence in the screening algorithm, while the stable observed {101} and {001} surfaces only occur 9.5% and 4.3% of the time, respectively. From the static calculated surface energies, the {112} surfaces are low enough to appear on the Wulff construction (Fig. 3), although they disappear when the surfaces are allowed to relax, and consequently the {101} and {001} surfaces dominate the morphology, as observed. This is because the (112) surfaces consists completely of 5-fold coordinated Ti atoms (Fig. 2d), while the (101) surface is mixed with fully 6-fold co-

Table 2
Heuristic screened anatase TiO_2 surfaces and resulting surface energies (in J/m^2).

Surface	Screening	γ_{static}	γ_{relax}
{112}	18%	1.40	0.75
{102}	15%	3.08	Unstable
{101}	10%	1.17	0.56
{104}	8.3%	2.58	1.48
{100}	6.7%	1.47	0.65
{001}	4.3%	1.07	0.92
{110}	1.5%	2.04	1.09

Fig. 3. Wulff construction of anatase TiO_2 from a.) static surface energies and b.) relaxed surface energies. The (112) surfaces are present on the particle morphology for the static surfaces, but relaxation greatly reduces the (101) surface energies relative to the (112) surfaces. (For interpretation of the references to color in this figure legend, the reader is referred to the web version of this article.).

ordinated and 5-fold coordinated Ti atoms. The surface energy of (001) is much higher than for the (101), but is still stable on the morphology, due to geometrical constraints in the Wulff construction.

Our screening heuristic additionally identifies, for the first time, the (102) and (104) surfaces, which are vicinal surfaces that occur in the azimuth between the (001) and (101) surfaces. While their surface energies are very high, and the (102) surface is actually dynamically unstable in DFT, the identification of these surfaces by our screening algorithm underscores the potential for these vicinal surfaces to be stabilized by capping agents from solution. Indeed, these surfaces are observed to become preferable to the (001) surface under high citric acid concentrations [32], although a calculation of these citric acid capped surfaces is outside the scope of this investigation. Nevertheless, the rich variety of surfaces screened for Anatase TiO_2 again highlights the potential for a variety of morphologies to be accessed by this structure.

4. Surface energy vs. chemistry

The corundum structure is the most common binary oxide structure in the A_2X_3 stoichiometry, forming seven compounds – the Group III semiconductor oxides Al_2O_3, Ga_2O_3, In_2O_3, as well as the transition metal oxides Ti_2O_3, V_2O_3, Cr_2O_3, and Fe_2O_3. This provides an excellent opportunity to investigate how surface energies trend with chemistry when structure is fixed, particularly because the Group III oxides descend vertically in the periodic table, while the transition metal oxides extend horizontally in the periodic table. Group III elements are also significantly less redox-active than the transition metals, which may affect how cleaved surfaces relax in response to bond-breaking. The corundum structure is the ground-state structure for all compounds except V_2O_3 and In_2O_3, where it is metastable with respect to bixbyite, and in Ga_2O_3, where the β-Ga_2O_3 phase is the ground-state. However, for these three chemistries, the corundum structure is still within a small enough enthalpy range of the ground-state to be accessible under applied thermodynamic conditions [33].

Despite minor differences in the atomic sizes and bond-lengths across the 7 isostructural oxides, the screening heuristic obtains the same surface orientations, shown in Fig. 1, for all chemistries. We focus our investigation on the four primary surfaces; the $\{10\bar{1}2\}$ surface, with 100%

5-fold coordinated cations; the $\{10\bar{1}1\}$ surface, with 50% 4-fold coordinated cations and 50% 5-fold coordinated cations; the $\{10\bar{1}4\}$ surface, with 100% 4-fold coordinated cations; and the $\{0001\}$ surface, which has 100% 6-fold coordinated *topped* with 3-fold coordinated cations.

In the Group III-oxides; Al_2O_3, Ga_2O_3 and In_2O_3; the overall surface energies scale with the electropositivity of the cation, in the order $\gamma_{Al_2O_3} > \gamma_{Ga_2O_3} > \gamma_{In_2O_3}$, as shown in Fig. 4. For a given structure, a more electronegative cation results in a stronger bulk cohesive energy. Because surface energy is the work associated with bond-breaking, the more cohesive a solid, the higher its corresponding surface energies. In general, the Group III-oxides follow the trend that lower surface cation coordinations lead to higher static surface energies, in the order $\gamma_{\{10\bar{1}2\}} > \gamma_{\{10\bar{1}1\}} > \gamma_{\{0001\}}$. However, the static surface energy is anomalously for the In_2O_3 $\{0001\}$ surface. The $\{0001\}$ surface has mixed 6-fold and 3-fold surface atoms, which suggests that indium has a smaller penalty for 3-fold coordination than aluminum and gallium. Upon relaxation, the $\{0001\}$ surface becomes significantly stabilized for all Group-III oxides, which is generally associated with a significant bond-contraction in the dangling 3-fold coordinated metal cation. In these Group-III oxides, where the cations are generally not redox active, surface cation coordination is a good predictor for relative surface energy between various facets.

We next investigate the surface energies of the first-row transition metal corundum oxides; Ti_2O_3, V_2O_3, Cr_2O_3, and Fe_2O_3, as shown in Fig. 4. The relative surface energies of both static and relaxed surfaces trend similarly between Ti_2O_3 and Fe_2O_3, and between V_2O_3 and Cr_2O_3. Surface energies of V_2O_3 and Cr_2O_3 generally increase monotonically with decreasing surface coordination. On the other hand, for Fe_2O_3 and Ti_2O_3 the 4-fold coordinated $\{10\bar{1}4\}$ surface and 3-fold coordinated $\{0001\}$ surface both have lower energies than for the mixed 5- and 4-fold coordinated $\{10\bar{1}1\}$ surface. To understand why Fe_2O_3 and Ti_2O_3 do not exhibit the same energy penalty for surface under-coordination as V_2O_3 and Cr_2O_3, it is instructive to consider the oxidation states of the stable bulk phases. In both the V-O and Cr-O system, V_2O_3 and Cr_2O_3 are the most reduced bulk oxides. This suggests that further reduction of surface V^{3+} or Cr^{3+} ions by oxygen under-coordination would be energetically undesirable. On the other hand, more reduced bulk oxides exist in both the Fe-O and Ti-O systems, as Fe^{2+} can be found in both Wustite ($Fe_{0.947}O$) and magnetite (Fe_3O_4), and titanium suboxides are known to exist in the reduced Magneli phases (Ti_nO_{2n-1}) down to Ti_1O_1. Because iron and titanium can both be reduced further from the 3+ oxidation state, this explains why under-coordinated Ti_2O_3 and V_2O_3 surfaces can still be low in energy. More generally, our results show that surface energies in transition metal oxides do not always have a direct relationship with surface coordination, and that the chemistry of the redox-active element can influence relative facet stability on the particle morphology.

In conclusion, surfaces identified using the topological screening heuristic are generally applicable across isostructural materials, although the relative surface energies between screened orientations are dependent on the chemistry. Notably, we find two important factors that influence surface energies as a function of chemistry: 1) the propensity of the cation to tolerate under-coordination, and 2) the ability of the cation to be further electrochemically reduced.

5. Screened low-energy surfaces of common binary oxides

Having established that screened surfaces can be generally applied across isostructural compounds, we run our screening heuristic on the 9 most common binary oxide structures in the Inorganic Crystal Structure Database (ICSD), shown in Table 3, with surface orientations ordered in decreasing sampling frequency. In the binary oxides, we find that the surface orientations with the highest atomic density do tend to be low-index surfaces, consistent with general intuition. In these relatively simple structures, the conventional unit cell is defined such that atoms typically occupy the high-symmetry positions, which are coin-
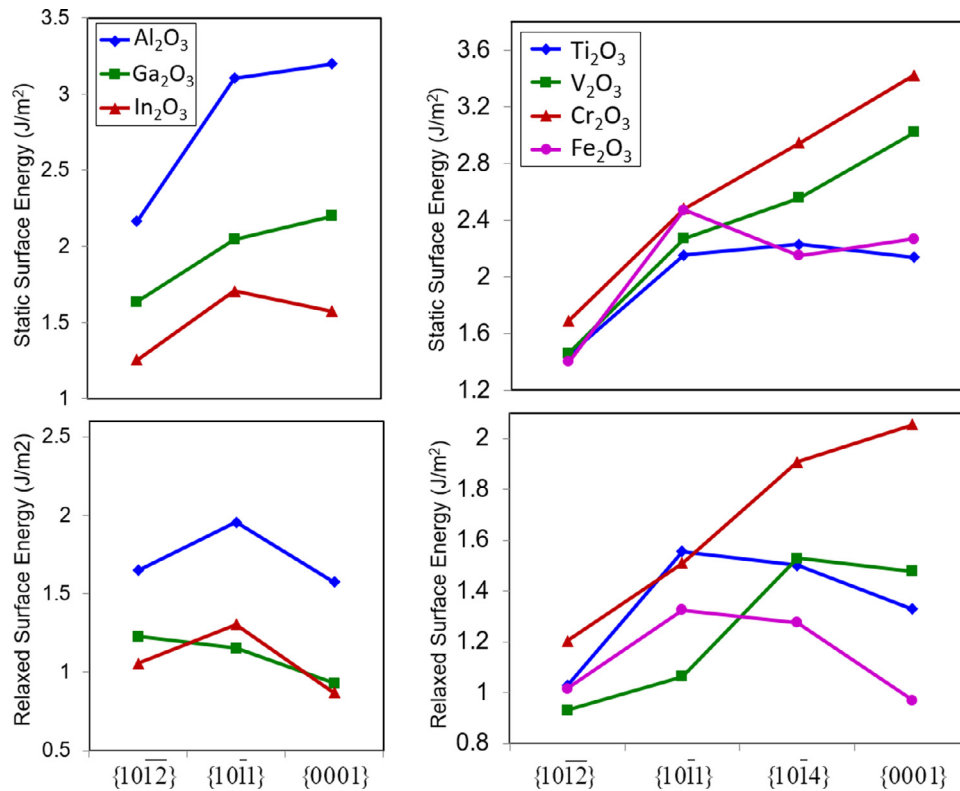
Fig. 4. Static and relaxed surface energies of the corundum structure with various cation chemistries. Left) the Group III-oxides, descending down the periodic table as Al, Ga, In. Right) The transition metal oxides, increasing in atomic number as Ti, V, Cr, and Fe.

Table 3
Screened surfaces for the 9 most common binary oxide structures.

Stoichiometry	Structure prototype	# ICSD entries	Competitive surface orientations				
AO	Rock salt (MgO)	21	{100}	{110}	{111}	{210}	{211}
AO_2	Rutile (TiO_2)	20	{101}	{100}	{110}	{111}	{001}
AO_2	PdF_2–Rutile (SnO_2)	9	{100}	{110}	{011}	{103}	{112}
A_2O_3	Corundum (Al_2O_3)	8	{10$\bar{2}$}	{104}	{2$\bar{1}$0}	{101}	{001}
AO_2	Fluorite (ZrO_2)	8	{100}	{100}	{110}	{111}	{210}
AO	ZnS-type (BeO)	6	{101}	{100}	{111}	{103}	{211}
AO_2	Peroxide (KO_2)	6	{101}	{110}	{001}	{103}	{112}
AO	Wurtzite (ZnO)	5	{001}	{101}	{2$\bar{1}$2}	{302}	{100}
A_2O	Cu_2O-type (Cu_2O)	5	{111}	{100}	{110}	{311}	{210}

cident with low Miller index orientations. This is especially apparent in the cubic, tetragonal, and orthorhombic crystal systems; as exemplified in the rock salt, rutile, fluorite, and Cu_2O prototype families. However, higher-index orientations are sampled more frequently in the non-orthorhombic structures, such as in rhombohedral corundum and hexagonal Wurtzite, as the occupied high-symmetry points do not always fall upon low-index orientations. For example, in Wurtzite ZnO (Space group $P6_3mc$), both Zn and O fall upon the 2b Wyckoff position, with coordinates (1/3, 2/3, z) and (1/3, 2/3, z + 1/2), so that our surface screening algorithm identifies the {2$\bar{1}$2} and the {302} surfaces, which have been observed in the facet evolution of nanowire tips [34]. Our algorithm identifies minority high-index surfaces for nearly all structures; these high-index surfaces can often be stabilized if a proper nanoparticle environment can be identified, such as the reducing environments previously discussed in the Cu_2O case.

6. Conclusion

We have thus contributed a simple and efficient heuristic to screen for low-energy surfaces, based on the intuition that planes with high atomic density tend to possess low surface energies. Our algorithm

searches for high-density planes based on atomic coordinates, rather than on the lattice, meaning that Miller index enumeration techniques are unnecessary to identify low-energy, high-index surfaces. We validated our algorithm over various binary oxide structures, showing that we not only identify high-index surfaces that are stable on the Wulff construction, such as the {10$\bar{1}$2} surface of corundum Al_2O_3, but also high-energy, high-index surface orientations that are stabilizable under specific nanoparticle environments, such as Anatase {112} and Cuprite {311}. Screened surfaces tend to be applicable across isostructural compounds, and we provided the surface screening results for the nine most common binary oxide structures in the Inorganic Crystal Structure Database.

In this work, we focused our investigation on the binary oxides, which have relatively simple structures. There are some opportunities for improving algorithm performance in more complicated crystal structures, while maintaining the same conceptual framework of the algorithm. In materials where there is polyhedral distortion or anisotropy, such as due to Jahn–Teller effects, one could include a tolerance for when an atom is considered to lie on a particular Miller plane. In materials with anion or cation complexes, such as CO_3^{2-} or NH_4^+, there may be clever coarse-graining approaches to describe the complex rather than

using the center atom as a single-point for screening. This would particularly be prudent in anions with irregular and extended polyhedral, such as $(P_3S_{11})^{7-}$ anions in $Li_3P_3S_{11}$ or $(Ge_2N_2)^{6-}$ in $Sr_3Ge_2N_2$.

Acknowledgements

Supplementary materials

Supplementary material associated with this article can be found, in the online version, at doi:10.1016/j.susc.2017.11.007.

References

[1] H.G. Yang, et al., Anatase TiO_2 single crystals with a large percentage of reactive facets, Nature 453 (7195) (2008) 638–641.

[2] K.A. Stoerzinger, et al., Orientation-dependent oxygen evolution activities of rutile IrO_2 and RuO_2, J. Phys. Chem. Lett. 5 (10) (2014) 1636–1641.

[3] H.G. Liao, et al., Facet development during platinum nanocube growth, Science 345 (6199) (2014) 916–919.

[4] L. Wang, et al., First-principles study of surface properties of $LiFePO_4$: surface energy, structure, Wulff shape, and surface redox potential, Phys. Rev. B 76 (16) (2007) 165435.

[5] J. Zhu, K.Y. Simon Ng, D. Deng, Micro single crystals of hematite with nearly 100% exposed {104} facets: preferred etching and lithium storage, Cryst. Growth Des. 14 (6) (2014) 2811–2817.

[6] W. Sun, et al., Nucleation of metastable aragonite $CaCO_3$ in seawater, Proc. Natl. Acad. Sci. 112 (11) (2015) 3199–3204.

[7] N. Tian, et al., Synthesis of tetrahexahedral platinum nanocrystals with high-index facets and high electro-oxidation activity, Science 316 (5825) (2007) 732–735.

[8] M. Leng, et al., Polyhedral 50-facet Cu_2O microcrystals partially enclosed by {311} high-index planes: synthesis and enhanced catalytic CO oxidation activity, J. Am. Chem. Soc. 132 (48) (2010) 17084–17087.

[9] R. Tran, et al., Surface energies of elemental crystals, Sci. Data 3 (2016).

[10] D.F. Cox, T.B. Fryberger, Steve Semancik, Surface reconstructions of oxygen deficient SnO_2 (110), Surf. Sci. 224 (1-3) (1989) 121–142.

[11] X.G. Wang, A. Chaka, Matthias Scheffler, Effect of the environment on $\alpha-Al_2O_3$ (0001) surface structures, Phys. Rev. Lett. 84 (16) (2000) 3650.

[12] K. Reuter, M. Scheffler, Composition, structure, and stability of RuO_2 (110) as a function of oxygen pressure, Phys. Rev. B 65 (3) (2001) 035406.

[13] W. Sun, G. Ceder, Efficient creation and convergence of surface slabs, Surf. Sci. 617 (2013) 53–59.

[14] P.E. Blöchl, O. Jepsen, O.K. Andersen, Improved tetrahedron method for Brillouin–zone integrations, Phys. Rev. B 49 (23) (1994) 16223.

[15] J.P. Perdew, K. Burke, M. Ernzerhof, Generalized gradient approximation made simple, Phys. Rev. Lett. 77 (18) (1996) 3865–3868.

[16] B. Meredig, et al., Method for locating low-energy solutions within DFT+ U, Phys. Rev. B 82 (19) (2010) 195128.

[17] S.P. Ong, et al., Python materials genomics (pymatgen): a robust, open-source python library for materials analysis, Comput. Mater. Sci. 68 (2013) 314–319.

[18] M. Kitayama, A.M. Glaeser, The Wulff shape of alumina: III, undoped alumina, J. Am. Ceram. Soc. 85 (3) (2002) 611–622.

[19] MTI Corporation, Al2O3- sapphire wafer, (10-14) orientation, product #AL(10-14)101005S1, retrieved from http://www.mtixtl.com/.

[20] J. Zhu, K.Y. Simon Ng, D. Deng, Micro single crystals of hematite with nearly 100% exposed {104} facets: preferred etching and lithium storage, Crys. Growth Des. 14 (6) (2014) 2811–2817.

[21] J.N. Kondo, Cu_2O as a photocatalyst for overall water splitting under visible light irradiation, Chem. Commun. 3 (1998) 357–358.

[22] W.-C. Huang, et al., Synthesis of Cu_2O nanocrystals from cubic to rhombic dodecahedral structures and their comparative photocatalytic activity, J. Am. Chem. Soc. 134 (2) (2011) 1261–1267.

[23] X. Wang, et al., A facile strategy for crystal engineering of Cu_2O polyhedrons with high-index facets, Cryst. Eng. Comm. 15 (10) (2013) 1849–1852.

[24] P.W. Tasker, The stability of ionic crystal surfaces, J. Phys. C 12 (22) (1979) 4977.

[25] A. Eichler, G. Kresse, First-principles calculations for the surface termination of pure and yttria-doped zirconia surfaces, Phys. Rev. B 69 (4) (2004) 045402.

[26] N.G. Hörmann, A. Groß, Polar surface energies of iono covalent materials: implications of a charge transfer model tested on Li2FeSiO4 Surfaces, ChemPhysChem 15 (10) (2014) 2058–2069.

[27] A. Fujishima, Electrochemical photolysis of water at a semiconductor electrode, Nature 238 (1972) 37–38.

[28] R.L. Penn, J.F. Banfield, Morphology development and crystal growth in nanocrystalline aggregates under hydrothermal conditions: Insights from titania, Geochimica et cosmochimica acta 63 (10) (1999) 1549–1557.

[29] M.R. Ranade, et al., Energetics of nanocrystalline TiO_2, Proc. Natl Acad. Sci. 99 (suppl 2) (2002) 6476–6481.

[30] A.S. Barnard, L.A. Curtiss, Prediction of TiO_2 nanoparticle phase and shape transitions controlled by surface chemistry, Nano Lett. 5 (7) (2005) 1261–1266.

[31] A. Testino, et al., Optimizing the photocatalytic properties of hydrothermal TiO_2 by the control of phase composition and particle morphology. A systematic approach, J. Am. Chem. Soc. 129 (12) (2007) 3564–3575.

[32] S. Yang, et al., Titania single crystals with a curved surface, Nature Commun. 5 (2014).

[33] W. Sun, et al., The thermodynamic scale of inorganic crystalline metastability, Sci. Adv. 2 (11) (2016) e1600225.

[34] X. Yin, X. Wang, Kinetics-driven crystal facets evolution at the tip of nanowires: a new implementation of the Ostwald–Lussac law, Nano Lett. 16 (11) (2016) 7078–7084.